Membrane Transport, Structure, Function, and Biogenesis:

Photoactivation of Channelrhodopsin

Oliver P. Ernst, Pedro A. Sánchez Murcia, Peter Daldrop, Satoshi P. Tsunoda, Suneel Kateriya and Peter Hegemann

J. Biol. Chem. 2008, 283:1637-1643.
doi: 10.1074/jbc.M708039200 originally published online November 9, 2007

Access the most updated version of this article at doi: 10.1074/jbc.M708039200

Find articles, minireviews, Reflections and Classics on similar topics on the JBC Affinity Sites.

Alerts:
- When this article is cited
- When a correction for this article is posted

Click here to choose from all of JBC's e-mail alerts

Supplemental material:
http://www.jbc.org/content/suppl/2007/11/14/M708039200.DC1.html

This article cites 30 references, 8 of which can be accessed free at
http://www.jbc.org/content/283/3/1637.full.html#ref-list-1

Downloaded from http://www.jbc.org/ at Duke University on December 6, 2013

THE JOURNAL OF BIOLOGICAL CHEMISTRY VOL. 283, NO. 3, pp. 1637–1643, January 18, 2008
© 2008 by The American Society for Biochemistry and Molecular Biology, Inc. Printed in the U.S.A.

Photoactivation of Channelrhodopsin*[S]

Received for publication, September 26, 2007, and in revised form, November 6, 2007 Published, JBC Papers in Press, November 9, 2007, DOI 10.1074/jbc.M708039200

Oliver P. Ernst[‡1], Pedro A. Sánchez Murcia[‡2], Peter Daldrop[§], Satoshi P. Tsunoda[§], Suneel Kateriya[¶], and Peter Hegemann[§3]

From the [‡]Institut für medizinische Physik und Biophysik, Charité-Universitätsmedizin Berlin, Charitéplatz 1, D-10117 Berlin, Germany, the [§]Institut für Biologie, Experimentelle Biophysik, Humboldt Universität zu Berlin, Invalidenstrasse 42, D-10115 Berlin, Germany, and the [¶]Department of Biochemistry, University of Delhi South Campus, Benito Juarez Road, New Delhi 110021, India

Channelrhodopsins (ChRs) are light-gated ion channels that control photomovement of microalgae. In optogenetics, ChRs are widely applied for light-triggering action potentials in cells, tissues, and living animals, yet the spectral properties and photocycle of ChR remain obscure. In this study, we cloned a ChR from the colonial alga *Volvox carteri*, VChR. After electrophysiological characterization in *Xenopus* oocytes, VChR was expressed in COS-1 cells and purified. Time-resolved UV-visible spectroscopy revealed a pH-dependent equilibrium of two dark species, D_{470}/D_{480}. Laser flashes converted both with $\tau \approx 200\ \mu s$ into major photointermediates P_{510}/P_{530}, which reverted back to the dark states with $\tau \approx 15–100$ ms. Both intermediates were assigned to conducting states. Three early intermediates P_{500}/P_{515} and P_{390} were detected on a ns to μs time scale. The spectroscopic and electrical data were unified in a photocycle model. The functional expression of VChR we report here paves the way toward a broader structure/function analysis of the recently identified class of light-gated ion channels.

The behavior of microalgae like *Chlamydomonas* is controlled by primordial eyes. The earliest events that are recorded from these eyes after light excitation are extremely fast photoreceptor currents (1–3) that are carried by Ca^{2+} and H^+ under most conditions (3, 4). The currents are generated by channelrhodopsins (ChRs),[4] microbial type rhodopsins with intrinsic ion conductance (5–7). ChRs gain their light sensitivity and gating properties from the covalently bound chromophore all-*trans*-retinal, which isomerizes after light absorption (8, 9). Studies in *Xenopus* oocytes and HEK293 cells revealed ChRs to be proton channels, which also conduct cations like Na^+, K^+, and Ca^{2+} (5, 6, 10). In these studies, light flashes evoked the ion conductance with a time constant of 200 μs after the flash, thus closely resembling the photocurrent rise in living algae (2, 6).

The observation that ChRs rapidly depolarize membranes within a few milliseconds in response to brief light flashes motivated neurophysiologists to use ChRs for controlling nerve cell firing. Originally, three groups in parallel expressed ChR in hippocampal neurons and triggered action potentials by short light pulses. The neurons followed the light stimulation protocols with action potential firing up to 30 Hz (10–12). ChR was also used to control neuronal activity in living animals, such as chicken embryos (11), *Caenorhabditis elegans* (13, 14), *Drosophila* (15), and mouse (16). In all cases, action potentials could be evoked by application of blue light to cells that were naturally light insensitive. The unique properties of ChR opened a new field of optogenetic technology for neuroscience and medical applications (17–19). However, despite the significant efforts that were made to make ChR available for such goals (20), the structure/function relationships of ChR, including the photoreactions as well as the ion channeling mechanism, remain unknown.

Here we describe the cloning and functional characterization of a ChR from the colonial alga *Volvox carteri* (VChR; see Fig. 1*A*). First, VChR was expressed in *Xenopus* oocytes and confirmed as a light-gated cation channel. Subsequently, it was expressed in COS-1 cells and functionally purified in detergent. This allowed us to obtain time-resolved UV-visible spectroscopic data and gain insight into the spectral properties and photocycle of this protein class. We identified two dark states and three photocycle intermediates with pH-dependent variations. Our studies on the transitions between the different states under various pH and light conditions are interpreted in a model that unifies the photocurrent kinetics and spectroscopic data.

EXPERIMENTAL PROCEDURES

Isolation and Cloning of the VChop DNA—Nucleotide sequences homologous to channelopsins Chop1 and Chop2 from *Chlamydomonas reinhardtii* were searched in a preliminary genome data base of *V. carteri* that is available within the *Chlamydomonas* genome project (genome.jgi-psf.org). *Chop* gene products are opsin apoproteins that form ChRs when reconstituted with the chromophore all-*trans*-retinal. Using the sequence information from the BLAST search, a 1797-bp fragment of the VChop cDNA was generated by reverse transcription-PCR from RNA isolated from a young *V. carteri* culture. See the supplemental data for details of cloning and

* This work was supported by Deutsche Forschungsgemeinschaft Grants Sfb 449 and Sfb 740 (to O. P. E.) and Sfb 498 (to P. H.). The costs of publication of this article were defrayed in part by the payment of page charges. This article must therefore be hereby marked "*advertisement*" in accordance with 18 U.S.C. Section 1734 solely to indicate this fact.

[S] The on-line version of this article (available at http://www.jbc.org) contains supplemental data.

[1] To whom correspondence may be addressed. Tel.: 49-30-450-524-111; Fax: 49-30-450-524-952; E-mail: oliver.ernst@charite.de.

[2] Recipient of an Erasmus fellowship from the European Commission, Spanish Ministerio Educación y Ciencia, and Universidad Complutense Madrid.

[3] To whom correspondence may be addressed. Tel.: 49-30-2093-8681; E-mail: hegemape@rz.hu-berlin.de.

[4] The abbreviations used are: ChR, channelrhodopsin; VChR, channelopsin from *V. carteri*; Chop, channelopsin; TM, transmembrane helix; dodecyl maltoside, *n*-dodecyl-β-d-maltoside; MOPS, 4-morpholinepropanesulfonic acid.

Downloaded from http://www.jbc.org/ at Duke University on December 6, 2013

sequence information on the resulting VChop cDNA fragment (GenBank™ accession number DQ094781).

Heterologous Expression in Xenopus Oocyte—A VChop cRNA fragment encoding $VChR_{1-307}$ (amino acids 1–307) was synthesized *in vitro* from NheI-linearized pGEMHE-plasmid (5, 6) by using T7 RNA polymerase (mMessage mMachine, Ambion). Oocytes prepared from female *Xenopus* (5, 6) were obtained from Ecocyte Bioscience and were injected with 50 nl of VChop cRNA fragment (0.5–1.0 μg/μl) and incubated in the dark at 18 °C in Ringer solution (96 mM NaCl, 5 mM KCl, 1.8 mM $CaCl_2$, 1 mM $MgCl_2$, 5 mM MOPS, pH 7.5) in the presence of 1 mg/ml penicillin, 1 mg/ml streptomycin, 0.5 mM theophylline, and 1 μM all-*trans*-retinal (Sigma).

Electrophysiology—Two-electrode voltage clamp measurements on *Xenopus* oocytes were performed 3–7 days after injection at 22 °C under the conditions described before (21, 22). For high resolution experiments a Turbo Tec-05X amplifier (NPI Electronic, Tamm, Germany) was used. The data obtained were normally the averages of three measurements. The resistances of microelectrodes were 0.5–1.5 MΩ. For recording of fast kinetics, 10-ns flashes (400–600 nm) from a Rainbow OPO (OPOTEK, Carlsbad, CA) pumped by the third harmonic of a Brilliant b Nd-YAG-Laser (Quantel, Les Ulis Cedex, France) were applied via a 1-mm light guide. The current amplifier Tec-05X was compensated so that the voltage change was kept below 1 mV at a half-saturating laser flash. The data were recorded at high gain with a sampling rate of 250 kHz. The laser intensity varied from flash to flash within a range of 5%. Bath solution was 100 mM NaCl, 0.1 mM $CaCl_2$, 0.1 mM $MgCl_2$ with 5 mM MOPS-NaOH, pH 7.5, or 5 mM citrate, pH 4.0. The conditions for light pulse experiments were 500 ± 5 nm, 2×10^{22} photons m^{-2} s^{-1}.

VChR Expression in COS-1 Cells—For expression in COS-1 cells (ATCC, CRL-1650), a human codon-optimized synthetic VChop DNA fragment (corresponding to amino acids 1–307 of the native protein, accession number DQ094781), plus the C-terminal ETSQVAPA sequence (1D4 epitope (23)) was designed and purchased from GeneArt (Regensburg, Germany). The synthetic VChop DNA was inserted between the EcoRI-NotI sites of the expression vector pMT3 (24). Tissue culture, transient transfection with the resulting VChR-pMT3 vector, reconstitution with chromophore, and subsequent purification of VChR was performed basically as described for bovine rhodopsin (25, 26). Three days after transfection, the cells were harvested and reconstituted with all-*trans*-retinal (final concentration, 1.5 μM). VChR was solubilized with dodecyl maltoside and purified by immunoaffinity adsorption using rho 1D4 antibody coupled to CNBr-activated Sepharose 4 Fast Flow (GE Healthcare). VChR was eluted with 100 μM of an 18-mer peptide corresponding to the C-terminal rhodopsin sequence in 0.03% (w/v) dodecyl maltoside, 10 mM 1,3-bis-[tris(hydroxymethyl)methylamino] propane, pH 6.0 (25, 26). Eluates were dialyzed and/or concentrated using Centricon YM-10 (Millipore) concentrators and stored at 4 °C or −40 °C. The mutant VChR-K252G was generated by site-directed mutagenesis (QuikChange kit; Stratagene). The mouse anti-rhodopsin monoclonal antibody rho 1D4 used for purification and Western blotting of VChR was purchased from the University of British Columbia (Dr. R. Molday). Purified VChR was deglycosylated with peptide-*N*-glycosidase F (Roche) according to the manufacturer's instructions.

Spectroscopy—For absorption spectroscopy and slow kinetics at 20 °C, a Cary 50 Bio spectrophotometer (Varian Inc.) with a spectral resolution of 2 nm was used. The samples were illuminated for 10 s with a blue Luxeon LED (Philips Lumileds, San Jose, CA) with a wavelength of 456 nm, 90 milliwatt cm^{-2}, 2×10^{21} photons m^{-2} s^{-1}. Transient spectroscopy was performed on a LKS.60 flash photolysis system (Applied Photophysics Ltd., Leatherhead, UK) at 22 °C. Excitation pulses (10 ns, 450 nm) were provided by a tunable Rainbow OPO/Nd-YAG-Laser laser system (see above). Laser energy was adjusted to 3.5 ± 0.16 mJ/shot. The instrument used a Xe-Lamp (150 W) as a monitoring light source, which was pulsed during short time experiments. Monochromators before and after the sample were set to spectral resolutions of 18.6 and 9.3 nm, respectively. For detection, a 1P28 photomultipier (Hamamatsu Photonics) was used, and the signal was recorded with an Infinium Oscilloscope (Agilent Technologies). 32,000 data points were recorded in each measurement and compressed by LKS.60 software to files of 500 data points. 50 of these points were recorded before and 450 after laser excitation. To avoid artifacts and scatter, only data points 60–500 were used for analysis. Data analysis was performed with Matlab 7.01 (The MathWorks, Natick, MA). Singular value decomposition of representative data sets was performed to identify significant components that were used for reconstruction of the three-dimensional spectra (see supplemental data). For measurements at pH 6, freshly prepared VChop was used. For experiments at pH 7.3 and 4.5, freshly prepared VChop was dialyzed and/or diluted with buffer containing 0.03% dodecyl maltoside, yielding 100 mM NaCl, 0.1 mM $CaCl_2$, 0.1 mM $MgCl_2$ with 10 mM MOPS, pH 7.3, or 10 mM citrate, pH 4.5, and the pH was measured thereafter. pH titration was performed with 20 mM buffer (citrate, pH 4.5–6; MOPS, pH 7; or Tris, pH 8) in 100 mM NaCl, 0.1 mM $CaCl_2$, 0.1 mM $MgCl_2$, 0.03% dodecyl maltoside.

RESULTS

Functional Studies on VChR in Xenopus Oocytes—In the past, ChRs from *Chlamydomonas* were difficult to express in standard expression systems like *Escherichia coli*, yeast, or COS cells (27). We therefore isolated a ChR-related cDNA from young *V. carteri* colonies (Fig. 1*A*). The cDNA encoded a large Volvox-ChR protein, VChR (599 amino acids), with seven transmembrane helices (TM) and a long C-terminal extension. We only studied the 7TM region of VChR (Fig. 1*B*) corresponding to amino acids 1–307 (see supplemental data) because earlier work on *Chlamydomonas* ChR1 and ChR2 (5, 6) showed that the long C-terminal extension had little influence on the ion conducting properties. In VChR-expressing *Xenopus* oocytes, light pulses evoked an initial transient current that relaxed toward a stationary plateau (steady state; τ_1 = 40–85 ms depending on the extracellular H^+ concentration (pH_o) and membrane voltage (Fig. 2*A*). The current increased with progressing negative voltage and with decreasing pH_o (Fig. 2, *A* and *B*), whereas the transient fraction of the current was particularly dominant at high pH_o and low negative or positive

Downloaded from http://www.jbc.org/ at Duke University on December 6, 2013

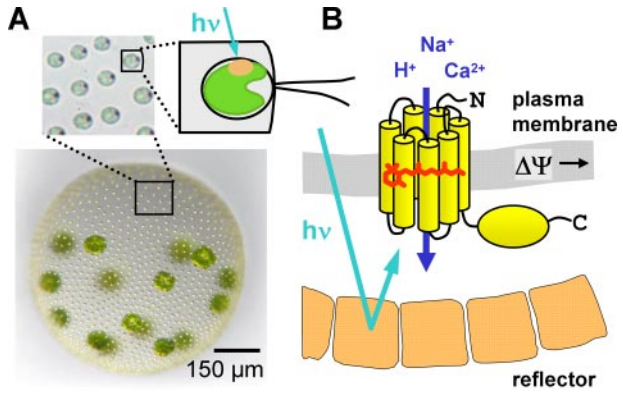

FIGURE 1. ***V. carteri.*** *A*, *Volvox* colony with a few thousand small *Chlamydomonas*-like somatic cells and 16 reproductive gonidia (courtesy of Armin Hallmann). The *inset* shows a few enlarged somatic cells with their red eyes. The cells at the surface of the colony with their flagella are shown schematically. *B*, VChR in the eye spot is a light-gated cation channel, which is composed of a seven transmembrane helix domain with the all-*trans*-retinal chromophore and a C-terminal tail of unknown function. Carotenoid-rich vesicles reflect the light and create a front to back contrast at the location of the ChR-photoreceptor. Absorption of light by VChR induces opening of the channel and thus changes of the membrane voltage.

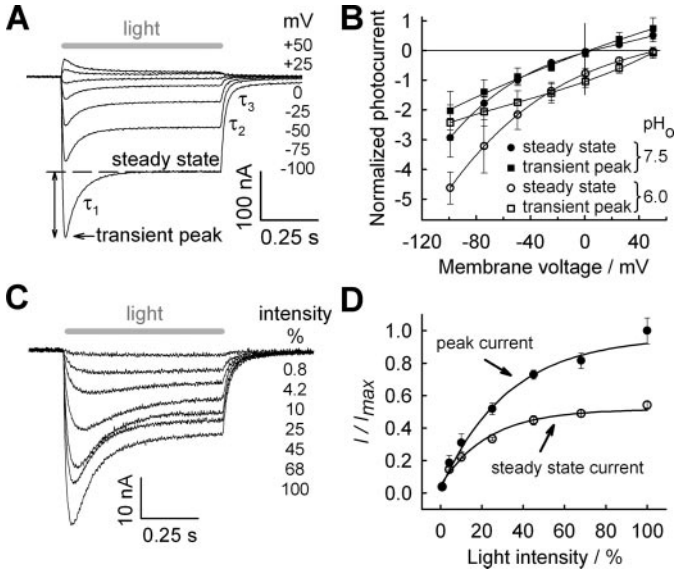

FIGURE 2. **Recordings of two-electrode voltage clamp from VChR-expressing *Xenopus* oocytes.** Voltage and light dependence of the VChR photoreceptor currents. *A*, photocurrents on VChR-expressing *Xenopus* oocytes measured with two-electrode voltage clamp in response to light pulses (indicated by a *gray bar*) ($\lambda = 500$ nm, 2×10^{22} photons $m^{-2} s^{-1}$) at seven different holding potentials. τ_1–τ_3 are time constants of the current decay as indicated. Bath solution contained 100 mM NaCl, 0.1 mM $MgCl_2$, 0.1 mM $CaCl_2$, and 5 mM MOPS-NaOH, pH 7.5. *B*, photocurrent/voltage (*I/V*) plot of the two photocurrent components; transient fraction (*squares*) and steady state fraction (*circles*). The data are averages from three independent experiments (*filled symbols*, pH_o 7.5; *open symbols*, pH_o 6.0). pH_o was adjusted to 6.0 with 5 mM citrate. *C*, photocurrents in response to various light intensities as indicated. 100% corresponds to 1.6×10^{22} photons $m^{-2} s^{-1}$. Bath solution was the same as in *A*. The membrane voltage was clamped at −100 mV. *D*, the (total) peak amplitude and the stationary level (at the end of the light pulse) of the photocurrents as shown in *C* are plotted as a function of light intensity (average of three experiments).

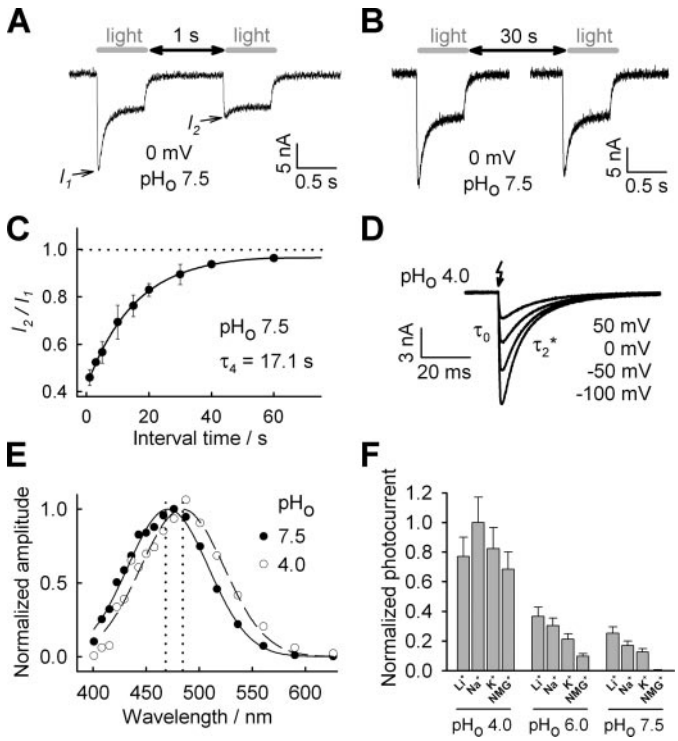

FIGURE 3. **Dependence of photocurrent on double light pulse stimulation, wavelength, and ionic conditions.** Two-electrode voltage clamp recordings from VChR-expressing *Xenopus* oocytes. *A*, two light pulses indicated as *gray bars* with 1-s dark interval evoke transient peak currents of different size but lead to similar stationary currents. *B*, almost full recovery of the second transient peak current is observed after a 30-s dark period. Bath solution contained 100 mM NaCl, 0.1 mM $MgCl_2$, 0.1 mM $CaCl_2$, and 5 mM MOPS-NaOH, pH 7.5. Membrane voltage was clamped at 0 mV. *C*, recovery of the second transient peak current (I_2) in relation to the first transient peak current (I_1) in double light pulse experiments as shown in *A* and *B*. *D*, photocurrent traces obtained by stimulation with 10-ns laser flashes ($\lambda = 470$ nm, membrane potential as indicated). *E*, action spectra resulting from stimulation with 10-ns laser flashes of various wavelengths at pH_o 7.5 and pH_o 4.0, peaking at 470 and 484 nm, respectively. The data points shown are averages of 20–25 recordings. *F*, cation selectivity measured under three different pH_o conditions with membrane potential at −100 mV. Bath solution contained 100 mM LiCl, NaCl, KCl or NMG-Cl with 0.1 mM $CaCl_2$, and 0.1 mM $MgCl_2$ plus 5 mM citrate (for pH 4.0 and 6.0) or 5 mM MOPS-NaOH (for pH 7.5). The currents were normalized to those recorded with NaCl and pH_o 4. The data shown are the averages of more than three independent experiments.

voltage values. After the light is off, the current decays biexponentially with $\tau_2 = 15$–25 ms and $\tau_3 = 60$–140 ms (−100 mV, pH_o 4–7.5).

The current amplitude certainly also depends on the light intensity, but the stationary current saturates at lower light intensities than the transient component (Fig. 2, *C* and *D*). Upon stimulation with two subsequent light pulses, the transient component of the second photocurrent is reduced in size (light adaptation; Fig. 3, *A* and *B*), and the recovery of the transient signal (dark adaptation) depends on the delay between the light pulses (Fig. 3*C*). The time constant (τ_4) of the transient recovery time is about 17 s at pH_o 7.5.

To further investigate the photocurrent kinetics, cells were stimulated with 10-ns laser flashes of 470-nm light (Fig. 3*D*). The photocurrent rose with a time constant (τ_0) in the range of 200 μs, and the current peaked at around 1 ms after the flash and relaxed to zero biexponentially with a dominant time constant τ_2^* (>90%) of about 16 ms at pH_o 7.5 and −100 mV. Repetitive laser flashes did not significantly promote light adaptation, which we considered as ideal for action spectroscopy. The normalized action spectrum recorded at pH_o 7.5 is rhodopsin-shaped with a half-bandwidth of 90 nm and a maximum at 470 nm (Fig. 3*E*). Interestingly, upon lowering the pH_o to 4,

Downloaded from http://www.jbc.org/ at Duke University on December 6, 2013

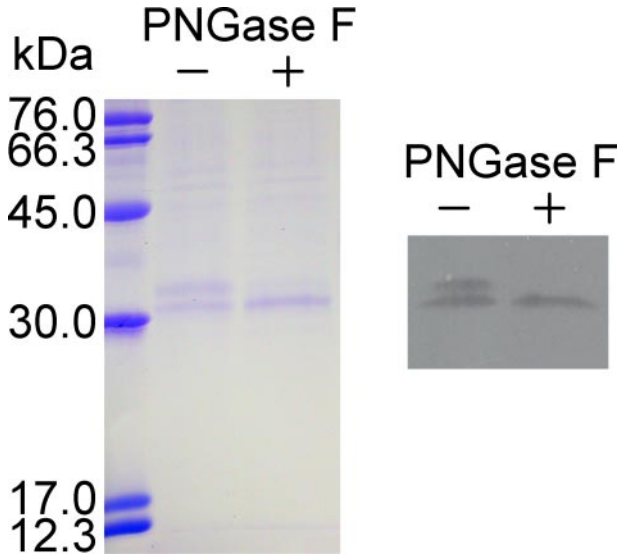

FIGURE 4. **Purified VChR.** SDS-PAGE (*left panel*) and Western blot (*right panel*; antibody: α-rho 1D4) of purified VChR before and after glucosidase PNGase F treatment are shown.

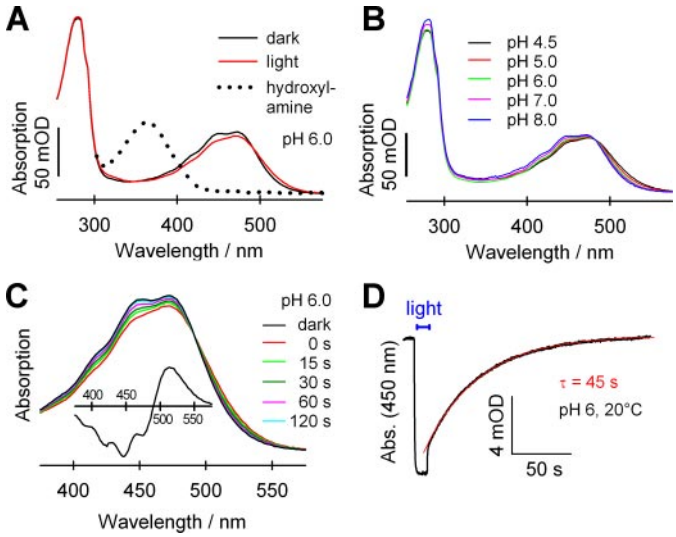

FIGURE 5. **UV-visible spectroscopy of purified VChR.** *A*, absorption spectra of purified VChR in dodecyl maltoside solution at pH 6 in the dark-adapted state (*black line*) and after 10 s of illumination with blue light (456 nm; *red line*). A 5-min incubation of VChR with 50 mM hydroxylamine in the dark led to formation of the apoprotein and retinaloxime (λ_{max} = 365 nm; *dotted line*). *B*, absorption spectra of dark-adapted VChR at different pH values, normalized at 482 nm. *C*, recovery of dark-adapted VChR. After illumination as in *A*, spectra were taken at times indicated. The calculated difference spectrum (*light minus dark*) was plotted on the same *x* axis (*inset*). *D*, recovery of dark-adapted VChR recorded at 450 nm corresponding to *C*.

the action spectrum was shifted to 484 nm, indicating two different dark states. We further determined that VChR is permeable for $H^+ \gg Li^+ > Na^+ > K^+$ (Fig. 3*F*) and poorly permeable for Ca^{2+} (≤10% of the Na^+ conductance) and is in this respect similar to its *C. reinhardtii* relative ChR2.

Spectroscopic Characterization of VChR—To get insight into the photocyle and the gating mechanism of VChR, spectroscopic measurements were performed with purified VChR. We used COS-1 cells to express the VChR 7TM region (amino acids 1–307; see supplemental data) plus nine additional amino acids corresponding to the C terminus of bovine rhodopsin (as epitope tag (23, 28) for purification and detection by protein immunoblotting). The expressed VChR was reconstituted with all-*trans*-retinal and purified by immunoaffinity chromatography in dodecyl maltoside solution. Fig. 4 shows the purified protein as a double band of 31 and 34 kDa on a SDS-PAGE (*left panel*) and after protein immunoblotting (*right panel*). The 34-kDa band disappeared after treatment with glucosidase (PNGase F), suggesting that the protein was partially glycosylated.

The spectrum of dark-adapted VChR at pH 6 showed an absorption with vibrational fine structure and two maxima at 450 and 470 nm, indicating a rigid chromophore with protonated retinal-protein Schiff base linkage (Fig. 5*A*). The absorption is sensitive to hydroxylamine, which extracts the retinal by formation of retinaloxime (*dotted line*) and allows determination of the molar extinction coefficient $\epsilon_{470} \approx 45.500\ M \cdot cm^{-1}$ (based on $\epsilon_{360} \approx 54.000\ M \cdot cm^{-1}$ for retinal oxime) (29). Lys-252 in TM7 was identified as the site of retinal attachment, because the K252G mutant did not show any absorption beyond 400 nm (data not shown). Acidification of the medium altered the shape of the VChR spectrum asymmetrically in favor of the long wavelength peak (Fig. 5*B*). The dark form observed at pH 8 was named D_{470}, whereas the acidic form was termed D_{480}. When the sample was illuminated at pH 6 with a blue LED (456 nm) for 10 s, the absorption again shifted slightly to the red (Fig. 5, *A*, *red versus black* spectrum, and *C*) in a similar manner as observed after acidification. Again, the absorption slightly declined, but in this case the shift was transient with $\tau \approx 45$ s at 20 °C (Fig. 5, *C* and *D*).

Next, purified VChR was excited with 10-ns laser flashes (450 nm), and absorption changes were recorded from 300 to 600 nm in 10-nm intervals up to 150 ms after the flash. At pH 7.3, the flashes initiated a fast absorption increase between 480 and 580 nm, which reached 90% of its maximal amplitude already at the first recorded time point (50 ns after the flash). Series of absorption difference spectra at pH 7.3 for the time ranges of 0.3–15 μs and 0.033–1.5 ms after the flash are shown in Fig. 6 (*A* and *B*, respectively). The three-dimensional spectra were reconstructed using significant components identified by singular value decompositon (see "Experimental Procedures"). The fastest occurring absorption difference maximum was found at 520 nm (Fig. 6*C*, *Early spectrum*), corresponding to an absolute maximum of the photoproduct near 500 nm. Accordingly, this early photocycle intermediate was named P_{500}. It converted with $\tau \approx 4$ μs into a species termed P_{390} (Fig. 6*A*) seen as an absorption difference peak between 370 and 380 nm in the transient spectrum (Fig. 6*C*, *Medium spectrum*). P_{390} decayed with $\tau \approx 200$ μs into a third photoproduct with an absorption difference maximum at 530 nm (Fig. 6, *B* and *D*, *Late spectrum*). This late intermediate was named P_{510} according to the estimated absolute absorption maximum.

At pH 4.5, flashes again initiated immediate absorption differences but with an early positive absorption difference peak at 535 nm (Fig. 6*E*), which is clearly red-shifted compared with the early photoproduct monitored at pH 7.3. The corresponding absorption maximum of the photoproduct is between 510 and 520 nm, and the species was termed P_{515} accordingly. The rise time was again below 100 ns. At later times the absorption dif-

Downloaded from http://www.jbc.org/ at Duke University on December 6, 2013

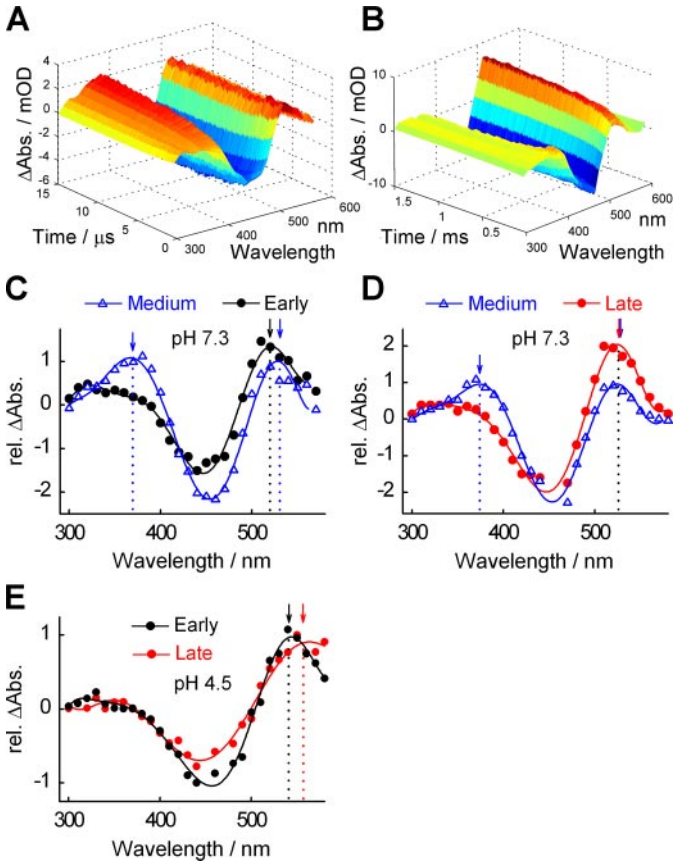

FIGURE 6. **Transient absorption difference spectra of purified VChR.** *A*, three-dimensional reconstruction of typical time-resolved absorption changes at pH 7.3 in the range from 0.3 to 15 μs after laser excitation. *B*, reconstructed spectra at pH 7.3 for the time interval 0.033–1.5 ms after flash. *C*, absorption differences resulting from *A*. The early intermediate P_{500} (*black circles*) is seen as the difference maximum at 520 nm (*arrow*; *Early spectrum*), whereas the two later intermediates P_{390} and P_{510} are seen as difference maxima at 370 and 530 nm, respectively (*blue triangles*; *Medium spectrum*). *D*, absorption differences resulting from *B*. Although the medium difference spectrum (*blue triangles*) comprises P_{390} and P_{510}, the late difference spectrum shows a single photocycle intermediate P_{510} only (*red circles*). *E*, absorption differences after a laser flash at pH 4.5. The early intermediate P_{515} (*black circles*) is seen as the difference maximum at 535 nm (*arrow*), whereas the late intermediate P_{530} is seen as difference maximum at 550 nm (*red circles*; *arrow*). The difference spectra result from two representative data sets: 0.25–59 μs after a flash (*Early spectrum*) and 0.15–7.5 ms (*Late spectrum*).

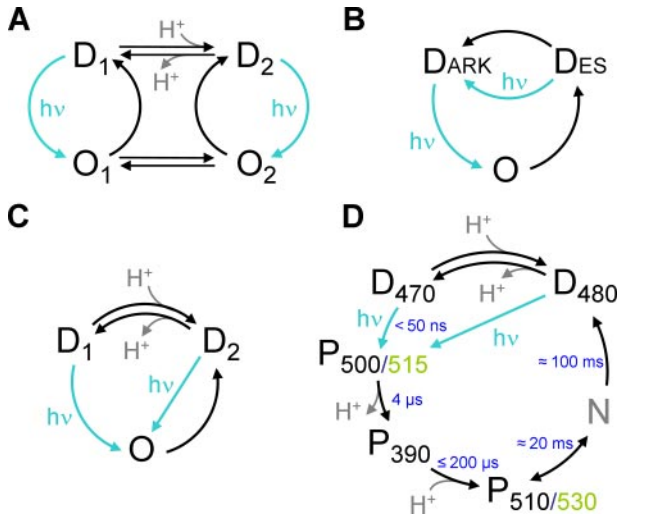

FIGURE 7. **Photocycle models.** *A*, four-state photocycle model originally derived from photocurrent measurements on ChR1 from *C. reinhardtii* (21). Two dark states, D_1 and D_2, as well as two photoactivated conducting states, O_1 and O_2, were proposed. A pH-dependent equilibrium of D_1 and D_2 was included to explain all of the photocurrent properties of VChR. *B*, three-state model according to Nikolic *et al.* (30) including one closed dark state Dark, one conducting state O, one desensitized state Des (closed without possibility to photoconvert to O), and an additional photoreaction from Des to Dark. *C*, three-state model comprising a pH-dependent equilibrium between two dark states, D_1 and D_2, and one conducting state that is reached with different efficiency from D_1 and D_2. *D*, photocycle scheme according to model *C* but including the two fast spectroscopically identified photocycle intermediates and indicating the absoption maxima. The acidic forms of the intermediates are shown in *green*; P_{510} and P_{530} are considered as conducting states; rough time constants (τ-values) are given in *blue*.

ference maximum shifted to ≈550 nm. This late species with a corresponding absorption maximum around 530 nm was named P_{530}. (Fig. 6*E*). Unfortunately, the resolution of our detection system and the smaller absorption changes under acidic conditions did not allow observation of the transition between P_{515} and P_{530}. Because no photoproduct equivalent to P_{390} was observed at pH 4.5, we conclude that only neutral conditions allow the formation or transient accumulation of a photoproduct with deprotonated retinal Schiff base during the VChR photocycle.

DISCUSSION

VChR Is Functionally Similar to Known ChRs from Chlamydomonas—We found that VChR from *V. carteri* is a functional relative of the two ChRs from *C. reinhardtii* with closer relation to ChR2. VChR shows electrical properties that are not explained by an earlier discussed three-state model with one closed dark state (Dark), one open state (O), one desensitized (closed and inactive) state (Des), and a single photochemical reaction from Dark to O (6). If the Des → Dark reaction is slow, at high light intensities most protein would be trapped in Des, and the stationary current would decay to zero. If the Des → Dark reaction is fast, the model fails to explain the slow recovery of the transient current. In contrast, all observed currents are fully consistent with the four-state model of Fig. 7*A* originally developed for ChR1 from photocurrent kinetics (21). It comprises two dark states, D_1 and D_2, and two conducting states, O_1 and O_2. On the basis of the present study, the model is extended by the pH dependence of the D1 ⇄ D2 equilibrium of dark-adapted VChR seen as a shift of the action spectrum (Fig. 3*E*). According to the four-state model, both D_1 and D_2 convert upon light excitation into separate conducting states, O_1 and O_2, that are also in equilibrium (21). At neutral pH, the O_2/O_1 ratio is assumed to be higher than the D_2/D_1 ratio, resulting in an accumulation of the weakly conducting state O_2 in the light and explaining the decay of the transient current to the stationary level. Nikolic *et al.* (30) quantitatively described the channelrhodopsin photocurrents by an extended three-state model (Fig. 7*B*) that was already considered earlier qualitatively (6). The "Nikolic model" assumes that the recovery of the Dark state from the (closed and desensitized) Des state is accelerated by light. The model is attractive because it describes the photocurrents adequately and involves less rate constants compared with the four-state model. The Nikolic model, however, does not explain the pH-induced shift of the action spectrum. Based on the electrical measurements and spectroscopic

Downloaded from http://www.jbc.org/ at Duke University on December 6, 2013

data generated for VChR, we are proposing here a photocycle (Fig. 7*C*) that is a hybrid of the four-state model (Fig. 7*A*) and the three-state Nikolic model (Fig. 7*B*). Because the acidic form and the preilluminated species (light-adapted VChR) are virtually identical, although there might be slight differences that are still unknown, we assume that D_{480} (D_2) is an intermediate of the photocycle starting from D_{470} (D_1). D_1 and D_2 are in a pH-dependent equilibrium, and both states are photoconverted into a conducting state O. The model converges with the four-state model by assuming a fast equilibrium between O_1 and O_2 (representing O) and a preferential thermal reaction from O to D_2 (D_{480}). A back reaction from O to D_1 (D_{470}) is not necessarily excluded but not explicitly needed for explaining the photocurrents. The transient nature of the current is explained in the model shown in Fig. 7*C* by a low quantum efficiency for the D_2 (D_{480}) to O transition rather than by a second conducting state. The three perspectives (Fig. 7, *A–C*) are kinetically quite equivalent and describe the photocurrents equally well (results of the calculations are available on demand). The assumption of a less efficient photoconversion of D_2 (D_{480}) is supported by the small light-induced absorbance changes observed at pH 4.5. Moreover, proteorhodopsin, a microbial rhodopsin from the noncultivated marine *γ-protobacterium*, shows a red-shifted absorption under moderately acidic conditions, and the photoisomerization is less efficient compared with that of the alkaline form (31). It is known that protonation of the retinal Schiff base counterion in microbial rhodopsins (Glu-118 in VChR) lowers the quantum efficiency of photochemical 13-*trans*- to *cis*-isomerization because of a rise of the C_{13}-C_{14} rotation barrier in the excited state (32). For VChR this results in a reduced stationary photocurrent as soon as the D_2/D_1 equilibrium increases during illumination. The different amplitudes of the transient and stationary current even at saturating light are alternatively explained by a late photocycle intermediate because it occurs in all other microbial rhodopsins. Formation and decay of a corresponding state N would be adjusted in such a way that under all conditions, less than 60% of VChR is trapped in N.

Photocycle of VChR—The UV-visible absorption spectra presented above give a first insight into the absorption properties of the dark states and photointermediates of channelrhodopsin. The pH-dependent spectral equilibrium between D_{470} and D_{480} suggests protonation of an amino acid residue in the retinal-binding pocket. This residue is accessible from the extracellular bulk phase because the shift can be induced by extracellular acidification in oocyte experiments. At pH 7.3 the dominant photoproduct P_{510} is assigned as the conducting state that is relevant under most physiological conditions. The equivalent under acidic conditions is P_{530}.

The spectroscopic observations on VChR and most electrophysiological data are summarized by an extended model as shown in Fig. 7*D* that is compatible with that of Fig. *7C*. It comprises two dark states in equilibrium ($D_{470} \rightleftarrows D_{480}$) and corresponding photoproducts. Starting from D_{470}, the photoproduct P_{510} (considered as the dominant conducting state) is populated sequentially via P_{500} and P_{390}. Because of the strongly blue-shifted absorption, P_{390} is assumed to be the only photoproduct with deprotonated retinal Schiff base. Based on the assumption that P_{510} is the conducting state at neutral pH, we conclude that the dark-adapted channel converts from the closed to the open state with $\tau \approx 200$ μs after light absorption (light gating). This value is compatible with the photocurrent rise, τ_0, of the VChR currents in *Xenopus* oocytes (Fig. 3*D*) and in the living alga (2, 4). At acidic pH, a species with deprotonated retinal Schiff base (P_{390}) is not observed, and light gating might be faster compared with alkaline pH conditions. The main intermediates P_{510} and P_{530} decay biphasically ($\tau_2 \approx 20$ ms and $\tau_3 \approx 100$ ms), indicating that there is a spectrally similar intermediate N.

The $D_{480} \rightarrow D_{470}$ transition functionally reflects the light-dark adaptation process $D_2 \rightarrow D_1$ as recorded by photocurrent measurements, even if the transient photocurrent recovers three times as fast as the slow recovery of D_{470} after illumination with a light pulse (Fig. 5, *C* and *D*). The difference could derive from experimental conditions. The spectral data were obtained with VChR in solution, whereas photocurrents were recorded from VChR in oocyte membranes at different internal and external pH. The transition from $D_2 \rightarrow D_1$ (and thus $D_{480} \rightarrow D_{470}$) is expected to be a two-step process as already proposed before (21) and possibly comprising an isomerization and deprotonation reaction.

The kinetic model presented in this study unifies electrophysiological data with spectral information and should help to interpret photocurrents recorded from intact algae under various physiological conditions. We expect that in algae a shift from D_1 to D_2 at low pH_o and/or high light intensities reduces the H^+ and cation influx and prevents major depolarization (3, 4).

Conclusion—The functional purification and spectroscopic characterization of VChR we report here represents a major step toward a detailed structure/function analysis of ChR. It opens the possibility of tailoring ChRs for neuroscience and medical applications. In analogy to the development of green fluorescent proteins with specific absorption/fluorescence properties, desired spectral and kinetic properties of ChR will be obtained by protein engineering and subsequent spectroscopic analysis. This will enable the application of new ChRs with distinct electrical and spectral properties to selected cell types in tissues or living animals to remotely stimulate nerves and to potentially restore color vision in mouse or even human retina (16, 20).

Acknowledgments—We thank B. Dick, J. Engelmann, D. Gradmann, R. Hagedorn, K. P. Hofmann, A. Koch, L. Lustres, M. Prigge, and M. Sommer for experimental support and discussion.

REFERENCES

1. Sineshchekov, O. A., Litvin, F. F., and Keszthelyi, L. (1990) *Biophys. J.* **57,** 33–39
2. Holland, E. M., Braun, F. J., Nonnengasser, C., Harz, H., and Hegemann, P. (1996) *Biophys. J.* **70,** 924–931
3. Ehlenbeck, S., Gradmann, D., Braun, F. J., and Hegemann, P. (2002) *Biophys. J.* **82,** 740–751
4. Braun, F. J., and Hegemann, P. (1999) *Biophys. J.* **76,** 1668–1678
5. Nagel, G., Ollig, D., Fuhrmann, M., Kateriya, S., Musti, A. M., Bamberg, E., and Hegemann, P. (2002) *Science* **296,** 2395–2398
6. Nagel, G., Szellas, T., Huhn, W., Kateriya, S., Adeishvili, N., Berthold, P.,

Downloaded from http://www.jbc.org/ at Duke University on December 6, 2013

Ollig, D., Hegemann, P., and Bamberg, E. (2003) *Proc. Natl. Acad. Sci. U. S. A.* **100,** 13940–13945
7. Sineshchekov, O. A., Jung, K. H., and Spudich, J. L. (2002) *Proc. Natl. Acad. Sci. U. S. A.* **99,** 8689–8694
8. Hegemann, P., Gärtner, W., and Uhl, R. (1991) *Biophys. J.* **60,** 1477–1489
9. Lawson, M. A., Zacks, D. N., Derguini, F., Nakanishi, K., and Spudich, J. L. (1991) *Biophys. J.* **60,** 1490–1498
10. Ishizuka, T., Kakuda, M., Araki, R., and Yawo, H. (2006) *Neurosci. Res.* **54,** 85–94
11. Li, X., Gutierrez, D. V., Hanson, M. G., Han, J., Mark, M. D., Chiel, H., Hegemann, P., Landmesser, L. T., and Herlitze, S. (2005) *Proc. Natl. Acad. Sci. U. S. A.* **102,** 17816–17821
12. Boyden, E. S., Zhang, F., Bamberg, E., Nagel, G., and Deisseroth, K. (2005) *Nat. Neurosci.* **8,** 1263–1268
13. Nagel, G., Brauner, M., Liewald, J. F., Adeishvili, N., Bamberg, E., and Gottschalk, A. (2005) *Curr. Biol.* **15,** 2279–2284
14. Zhang, F., Wang, L. P., Brauner, M., Liewald, J. F., Kay, K., Watzke, N., Wood, P. G., Bamberg, E., Nagel, G., Gottschalk, A., and Deisseroth, K. (2007) *Nature* **446,** 633–639
15. Schroll, C., Riemensperger, T., Bucher, D., Ehmer, J., Voller, T., Erbguth, K., Gerber, B., Hendel, T., Nagel, G., Buchner, E., and Fiala, A. (2006) *Curr. Biol.* **16,** 1741–1747
16. Bi, A., Cui, J., Ma, Y. P., Olshevskaya, E., Pu, M., Dizhoor, A. M., and Pan, Z. H. (2006) *Neuron* **50,** 23–33
17. Zhang, F., Wang, L. P., Boyden, E. S., and Deisseroth, K. (2006) *Nat. Methods* **3,** 785–792
18. Herlitze, S., and Landmesser, L. T. (2007) *Curr. Opin. Neurobiol.* **17,** 87–94
19. Hausser, M., and Smith, S. L. (2007) *Nature* **446,** 617–619
20. Abbott, A. (2007) *Nature* **446,** 588–589
21. Hegemann, P., Ehlenbeck, S., and Gradmann, D. (2005) *Biophys. J.* **89,** 3911–3918
22. Tsunoda, S. P., Ewers, D., Gazzarrini, S., Moroni, A., Gradmann, D., and Hegemann, P. (2006) *Biophys. J.* **91,** 1471–1479
23. Molday, R. S., and MacKenzie, D. (1983) *Biochemistry* **22,** 653–660
24. Franke, R. R., Sakmar, T. P., Oprian, D. D., and Khorana, H. G. (1988) *J. Biol. Chem.* **263,** 2119–2122
25. Meyer, C. K., Böhme, M., Ockenfels, A., Gärtner, W., Hofmann, K. P., and Ernst, O. P. (2000) *J. Biol. Chem.* **275,** 19713–19718
26. Fritze, O., Filipek, S., Kuksa, V., Palczewski, K., Hofmann, K. P., and Ernst, O. P. (2003) *Proc. Natl. Acad. Sci. U. S. A.* **100,** 2290–2295
27. Sineshchekov, O. A., and Spudich, J. L. (2006) in *Handbook of Photosensory Receptors* (Briggs, W. R., and Spudich, J. L., eds) pp. 25–42, Wiley-VCH Verlag GmbH & Co.
28. MacKenzie, D., Arendt, A., Hargrave, P., McDowell, J. H., and Molday, R. S. (1984) *Biochemistry* **23,** 6544–6549
29. Groenendijk, G. W., de Grip, W. J., and Daemen, F. J. (1979) *Anal. Biochem.* **99,** 304–310
30. Nikolic, K., Degenaar, P., and Toumazou, C. (2006) in *Proceedings of the 28th IEEE EMBS Annual International Conference* Engineering in Medicine and Biology Society, Aug. 30–Sept. 3, 2006, New York, pp. 1626–1629
31. Huber, R., Kohler, T., Lenz, M. O., Bamberg, E., Kalmbach, R., Engelhard, M., and Wachtveitl, J. (2005) *Biochemistry* **44,** 1800–1806
32. Song, L., El-Sayed, M. A., and Lanyi, J. K. (1993) *Science* **261,** 891–894

Downloaded from http://www.jbc.org/ at Duke University on December 6, 2013